OXFORD CDE

Journal of Computational Design and Engineering, 2022, **9**, 1–13

DOI: 10.1093/jcde/qwac062
Advance access publication date: 25 July 2022
Research Article

Constructing foldable cylindrical surfaces via unfolded waterbomb origami units

Yan Zhao [1,*], Yinglei Wei[1], Yiyang Jia[2], Shiling Li[1], Mingyue Zhang[1], Lanling Zeng[1], Yang Yang[1] and Jun Mitani[3]

[1]School of Computer Science and Communication Engineering, Jiangsu University, 301 Xuefu Road, Zhenjiang, Jiangsu Province 212013, China
[2]Faculty of Science and Technology, Seikei University, Musashino, Tokyo 1808633, Japan
[3]Graduate School of Systems and Information Engineering, University of Tsukuba, Tsukuba, Ibaraki Prefecture 3050006, Japan
*Corresponding author. E-mail: yanzhao_cs@ujs.edu.cn

Abstract

Origami tessellations have shown the potential to be utilized for approximating curved target surfaces by folding a set of elemental units. As those units are in partially folded states, the origami approximation captures the outline of the target while demonstrating a corrugated surface. In this paper, we focus on the cylindrical surface and propose a method for constructing its discrete version via square or rectangular units with crease patterns inspired by the waterbomb tessellation. We unify the unit size through optimization to realize cost-efficient constructions. Three-dimensional curved structures are deployed by folding collinear creases between adjacent rows of units and the other creases in each row are remained unfolded. The deployed structure can still be folded to a compact state by folding all creases. To flexibly approximate the outline of the target surface, we analyse relationships between the width and height of the rectangular unit and utilize variations of the waterbomb tessellation to control the region of the origami structure when fully folded. The proposed method provides a novel solution to the so-called inverse-origami-design problem for generating foldable cylindrical surfaces using unfolded waterbomb origami units.

Keywords: computational origami, cylindrical surface approximation, waterbomb tessellations, foldable structures

1 Introduction

Origami, an ancient oriental art of paper folding, has been utilized to construct three-dimensional (3D) structures by folding two-dimensional (2D) flat sheet materials with designed crease patterns. One origami structure required to satisfy the developable constraint can be fabricated on a plane without cutting, which is attractive for manufacturing (Pérez & Suárez, 2007). The origami structure can still be flat-folded (Zhao *et al.*, 2017, 2018c), which is intriguing for effective storage and transportation. Furthermore, benefiting from the scale-independent feature, one preliminary prototype of origami can potentially be applied to applications whose size ranges from nano scale (Dey *et al.*, 2021), decimetre scale (Zhao *et al.*, 2018a), metre scale (Melancon *et al.*, 2021), to macro scale (Pehrson *et al.*, 2020).

Approximating a given target structure by folding a modified crease pattern is the so-called inverse design in origami. Tachi proposed the 'Origamizer' method which can obtain crease patterns for folding any polyhedron-based structures (Tachi, 2009, 2010b; Demaine & Tachi, 2017). A design method was proposed to interactively construct a 3D freeform surface which can be folded from a flat sheet (Tachi, 2010a). Origami tessellations consisting of a set of elemental units have also shown a potential way of constructing given target surfaces. Specifically, a system was developed for constructing target surfaces via generalized Resch's pattern (Tachi, 2013). Dudte *et al.* proposed solutions for fitting target surfaces based on modified Miura cells (Dudte *et al.*, 2016, 2021). Dang *et al.* proposed an inverse-design method involving two-stage optimization via Miura-ori (Dang *et al.*, 2022). Zhao *et al.* proposed a method for approximating target surfaces based on developable waterbomb tessellations (Zhao *et al.*, 2018b).

Constructing a given cylindrical surface via origami is a simple case of the inverse-origami-design problem, because its Gaussian curvature is zero. Such cylindrical origami structures have also drawn much attention from researchers and engineers and can potentially be applied to many practical uses, such as biomedical foldable stents (Kuribayashi *et al.*, 2006), tunable mechanical memory structures (Yasuda *et al.*, 2017), and deployable booms in space (Schenk *et al.*, 2014). The design and foldability of Miura-based cylindrical origami structures were studied (Wang *et al.*, 2016; Du *et al.*, 2021). Design methods for cylindrical together with axisymmetric structures via Miura-ori (Hu *et al.*, 2019) and waterbomb tessellations (Zhao *et al.*, 2021) were proposed. Note that the origami structures obtained from most design methods are in partially folded states when deployed. Even though a finer approximation corresponding to the target surface could be generated by increasing the number of units used to compose the crease pattern, such an origami approximation still demonstrates a corrugated surface.

However, from the viewpoint of generating a cylindrical surface, a natural way could be from bending a flat sheet material otherwise folding origami patterns consisting of periodic units, e.g., the Miura-ori and waterbomb tessellation. Such an obtained structure demonstrates a "smooth" surface which could be of vital importance for appearance design in engineering-

Received: March 7, 2022. **Revised:** July 6, 2022. **Accepted:** July 11, 2022

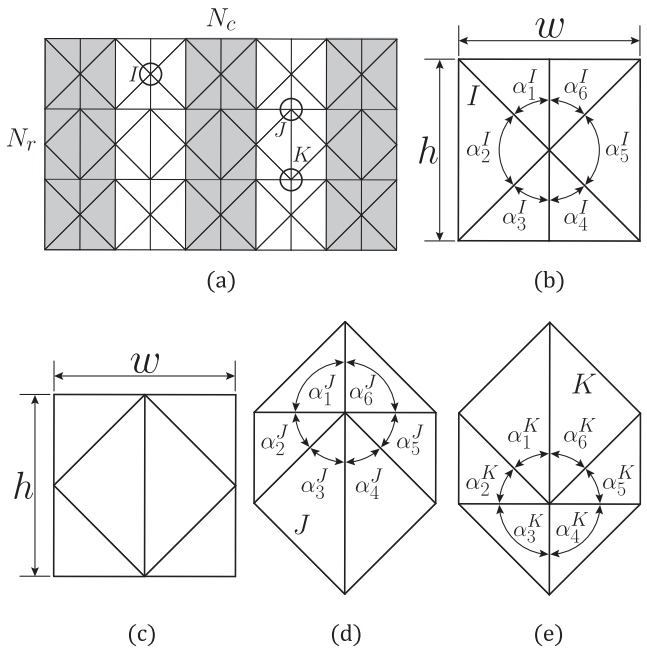

Figure 1: An introduction to the waterbomb tessellation. (a) A waterbomb tessellation consisting of $N_r \times N_c$ waterbomb bases, where $N_r = 3$ and $N_c = 5$ indicate the number of rows and columns, respectively. (b) A waterbomb base with equivalent width w and height h belongs to vertex type I. Such a unit, termed as U^O, is used to tile odd rows. (c) A shape obtained from the waterbomb base with swapping the left and right parts. Such a unit, termed as U^E, is adopted to tile even rows. (d) Vertex of type J and its surrounding angles. (e) Vertex of type K and its surrounding angles.

specific scenarios, e.g., the surfaces of a shelter and an airfoil require rain and airflow easily pass through. However, the deployed structure from bending may not be transformed to a compact state.

Recently, several studies have shown a research direction of constructing foldable origami structures with unfolded creases. Specifically, Melancon *et al.* utilized discrete panels to develop an inflation-actuated tent-like foldable structure (Melancon *et al.*, 2021). Sharma *et al.* constructed flat-foldable conical structures by using unfolded derivative Miura-ori (Sharma & Upadhyay, 2021). Tang *et al.* applied the waterbomb tessellation consisting of unfolded six-crease bases to generate discrete surfaces of revolution (Tang *et al.*, 2021).

We follow this research direction and propose an approach for constructing foldable cylindrical surfaces via square or rectangular units with crease patterns inspired by the waterbomb tessellation. The unit is one basic element, which is unified through optimization in terms of width w and height h. Thus, we could realize cost-efficient constructions (Lee *et al.*, 2022) for origami structures that are assembled by a large number of units required to be made individually. The generated crease pattern is developable and can be manufactured on a piece of flat sheet material without extra cutting. For approximating the cylindrical target surface from the 2D crease pattern, collinear creases between adjacent rows are folded simultaneously and appropriately like one hinge (Fig. 1a), while the creases in each row are remained unfolded. Such an approximation can be interpreted as a discrete version of the cylindrical target surface and can still be compactly stored by folding all creases. Besides the unit whose $w = h$, we investigate how two other relationships between w and h, i.e., $w < h$ and $w > h$, can affect the foldability of the deployed structure and introduce variations of the waterbomb tessellation for fitting the target surface.

The paper is organized as follows. Section 2 presents the approximating methodology inspired by waterbomb tessellations with square units in detail. Section 3 introduces variations of the waterbomb tessellation for approximation. Section 4 demonstrates results and Section 5 makes a discussion. Section 6 concludes the paper and points out future work.

2 Approximating Methodology Based on Square Units

In this section, we first introduce the waterbomb tessellation consisting of square bases and show the mechanism of constructing a cylindrical surface through bending a portion of creases. Then, we demonstrate an inverse-design framework for approximating given cylindrical target surfaces.

Figure 1a demonstrates a waterbomb tessellation containing $N_r \times N_c$ waterbomb bases, where $N_r = 3$ and $N_c = 5$ indicate the number of rows and columns, respectively. The waterbomb base with square shape whose width w is equivalent to height h (Fig. 1b) is mirror symmetric with respect to the central vertical edge. Six creases meet at one interior vertex which equally divides the vertical edge. By swapping the left and right parts of the base, a shape shown in Fig. 1c is obtained. As such a shape is consisting of a right and a left halves of the waterbomb base, it is considered as one waterbomb base for accounting. For obtaining the whole crease pattern, the waterbomb base termed as unit U^O (Fig. 1b) is utilized for tiling odd rows. To fit the upper boundary of odd rows, the shape termed as unit U^E (Fig. 1c) is adopted for tiling even rows.

We utilize angular relationships of each interior vertex to define geometric constraints, i.e., developability and flat-foldability. Based on the types of spherical 6R linkages (Feng *et al.*, 2018), interior vertices are classified as vertices I, J, and K shown in Fig. 1b, d, and e, respectively. Angle α_i, where $i = 1, 2, \ldots, 6$ in counterclockwise order, is introduced indicating the sector angle of one interior vertex. Because of the mirror symmetric, $\alpha_1 = \alpha_6$, $\alpha_2 = \alpha_5$, and $\alpha_3 = \alpha_4$. For expository purposes, we consider the angular relationship around vertex of type I as an example (Fig. 1b), where $\alpha_1^I = \alpha_3^I = \alpha_4^I = \alpha_6^I = \pi/4$ and $\alpha_2^I = \alpha_5^I = \pi/2$. Therefore, the sum of angles around the vertex of type I is equal to 2π, i.e.,

$$\alpha_1^I + \alpha_2^I + \ldots + \alpha_6^I = 2\pi,$$

satisfying the developable constraint (Demaine & O'Rourke, 2007). In addition, the sum of alternating angles around the vertex of type I equals π, such as,

$$\alpha_1^I + \alpha_3^I + \alpha_5^I = \alpha_2^I + \alpha_4^I + \alpha_6^I = \pi,$$

meeting the flat-foldable constraint (Demaine & O'Rourke, 2007). Similarly, for interior vertices of types J (Fig. 1d) and K (Fig. 1e), it is trivial to demonstrate the satisfaction of developability and flat-foldability. One waterbomb tessellation consisting of interior vertices of types I, J, and K is developable. Such an origami is flat-foldable if no self-penetration occurs during folding.

Among the creases of the waterbomb tessellation, it is observed that creases between adjacent rows are collinear, and thus can be folded simultaneously to act as one hinge (Fig. 1a). When folding each hinge appropriately, an origami structure corresponding to a given cylindrical target surface can be obtained. Angular relationships of each interior vertex are not altered, and thus the

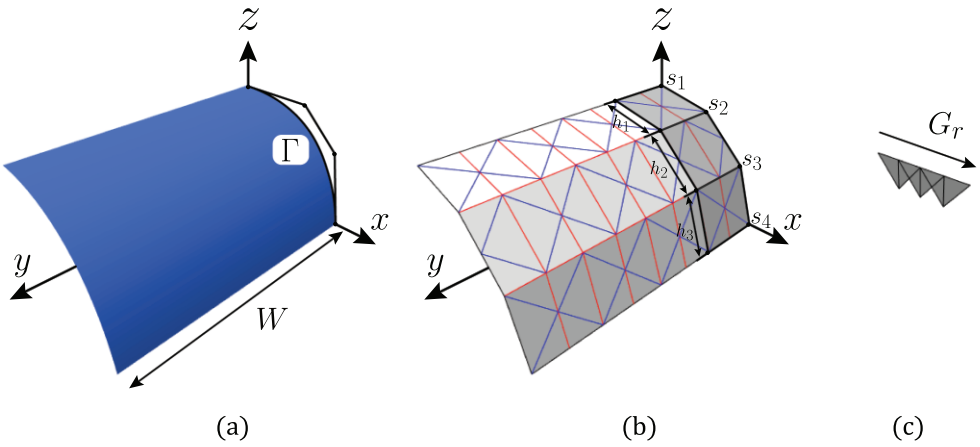

Figure 2: Approximating a cylindrical target surface using units of case $\mathbb{E}$. (a) A cylindrical target surface Φ^T specified by sweeping curve Γ lied on the x–z plane along the y-axis with a distance of W. (b) Tiling unfolded square units of case $\mathbb{E}$ on the target surface. (c) The flat-folded state of the origami approximation.

geometric constraints, i.e., developability and flat-foldability, are maintained.

We incorporate such an approximating mechanism into an inverse-origami-design framework. By utilizing the work of Zhao *et al.* (2021), a cylindrical target surface Φ^T (Fig. 2a) is firstly obtained by sweeping a 2D curve Γ on the x–z plane along the y-axis with a distance of W. In this work, Γ is represented by non-uniform rational basis spline (NURBS) curve, whose weights are all one and degree is set to three. The profile curve Γ together with the distance parameter W can be interactively designed to satisfy application-specific requirements of the appearance. With consideration of the periodic repetitions of columns, we focus on the column shaded in grey (Fig. 2b). Γ is divided into $N_r + 1$ sampling vertices, i.e., s_j where j ranges from 1 to $N_r + 1$, to form N_r segments. A straightforward way of division is to evenly sample $u \in [0, 1]$ of NURBS curve in parametric space. Besides, there exists another division strategy for minimizing the error between N_r segments and the curve based on Douglas–Peucker algorithm (Douglas & Peucker, 1973). Based on the above two division strategies, the lengths of the k th segment h_k, where k is from 1 to N_r, could be different, which potentially increases the difficulty and cost of fabrication especially when an origami structure is assembled by a large number of units required to be made individually. Here, we utilize the division strategy of unifying each length and introduce a length residual r_k defined as follows:

$$r_k = \frac{h_k - \overline{h}}{\overline{h}}, \tag{1}$$

where $\overline{h}$ is the average of all segment lengths in one column. Then, we formalize the following objective function:

$$E = \frac{1}{2}\sum_{k=1}^{N_r} r_k^2. \tag{2}$$

During the above optimization vertex s_j is perturbed for minimizing Equation (2). Coordinates x, y, and z, as one option, could be used as unknown parameters during optimization. However, extra efforts are needed to control the displacement of the sampling vertices from curve Γ. Instead, we utilize parameter u of every sampling vertex to let those sampling vertices glide along curve Γ for minimization. Starting and ending vertices can be fixed to keep the boundary of curve Γ. Under this option of choosing parameters, all sampling vertices are attached to Γ, and thus its outline is maintained. Without specific distinguishing, h is referring to $\overline{h}$ after optimization.

We simply set w as h and yield the origami approximation (Fig. 2b) consisting of unified square units with the waterbomb tessellation. Such square units (Fig. 1b and c) are termed as case $\mathbb{E}$. Mountain and valley assignments depicted in red and blue, respectively, can be utilized to guide the folding process. Under the zero-thickness material assumption, the deployed state is flat-folded into a 2D shape (Fig. 2c). We observe that the flat-folded shape is growing along a line when adding more square units by increasing N_r. Such a growing line is termed as G_r related to N_r. We place the flat-folded shape in the x–z plane and let its G_r be parallel to the x-axis. To evaluate the region of the flat-folded state, we calculate its axis-aligned bounding box (AABB). One square unit is flat-folded into an isosceles right triangle whose AABB has an area of $\frac{w}{2}h$. The whole structure is flat-folded into a region whose area of the AABB is

$$\begin{aligned} A^{\mathbb{E}} &= \frac{w}{2}\left(N_r h - (N_r - 1)\frac{h}{2}\right) \\ &= \frac{(N_r + 1)}{4} wh = \frac{(N_r + 1)}{4} h^2. \end{aligned} \tag{3}$$

The units of case $\mathbb{E}$ whose w is set by h, however, may not work well for application-specific approximating problems. Because the approximation width wN_c could be less or greater than the width W of the target surface Φ^T. To circumvent this limitation, we present details on $w < h$ and $w > h$ in the next section.

3 Approximating Methodology Based on Non-Square Units

In the previous section, the origami approximation consisting of unified square units with the waterbomb tessellation is obtained. In this section, instead of setting w as h for obtaining square units, w is set as W/N_c for fitting the width of the target surface. Therefore, w could be less or greater than h to form non-square units. We analyse how the relationships between w and h could affect the flat-folded state at first. Then, we introduce variations of the waterbomb tessellation for approximation.

For the 'tall' rectangular units whose $w < h$ (Fig. 3a and b), we obtain an approximation as shown in Fig. 3c. According to the

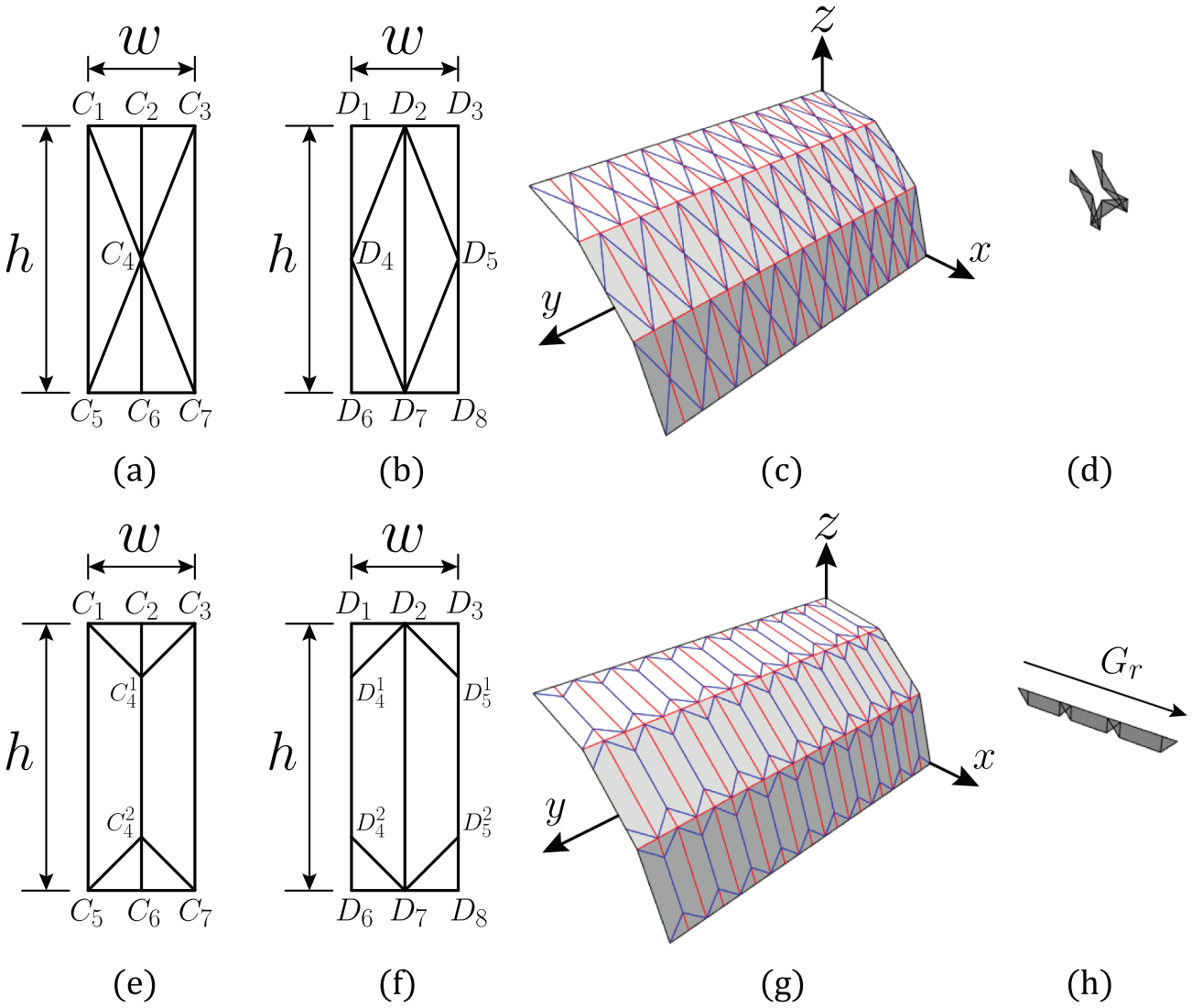

Figure 3: Cylindrical target surface approximation via rectangular units whose width w is less than height h. (a) A 'tall' rectangular unit U^O for tiling odd rows. (b) A 'tall' rectangular unit U^E for tiling even rows. (c) The approximated origami structure composed of units U^O and U^E. (d) The flat-folded state of the approximation shown in (c). (e) A unit U^O of case $\mathbb{T}$ modified from the unit shown in (a). (f) A unit U^E of case $\mathbb{T}$ modified from the unit shown in (b). (g) The approximated origami structure via units U^O and U^E of case $\mathbb{T}$. (h) The flat-folded state of the approximation shown in (g).

mountain and valley assignments, such an approximation could fold to reach a flat-folded state if no self-penetration among different parts of the structure occurs. Without further control, the outline of the flat-folded shape would be curved (Fig. 3d) which could generate a flat shape with self-overlaps. Inspired by the observation that the flat-folded shape based on units of case $\mathbb{E}$ is growing along a straight line (Fig. 2c), we modify the creases of tall units as shown in Fig. 3e and f. Specifically in modified unit U^O (Fig. 3e), the middle vertex C_4 is split into vertices C_4^1 and C_4^2 at the central line, letting edges $C_4^1C_2 = C_4^2C_6 = \frac{w}{2}$. Similarly, in modified unit U^E (Fig. 3f), D_4 is split into vertices D_4^1 and D_4^2, D_5 is split into vertices D_5^1 and D_5^2 to generate edges $D_4^1D_1 = D_4^2D_6 = D_5^1D_3 = D_5^2D_8 = \frac{w}{2}$. We term modified units U^O (Fig. 3e) and U^E (Fig. 3f) as case $\mathbb{T}$. The approximation containing such units and its corresponding flat-folded shape are shown in Fig. 3g and h, respectively. We place the flat-folded shape in the x–z plane and let its growing line G_r be parallel to the x-axis. The area of the AABB for the whole flat-folded shape is a slim rectangle, whose area is

$$A^{\mathbb{T}} = \frac{w}{2}\left(N_r h - (N_r - 1)\frac{w}{2}\right) = \frac{2N_r wh - N_r w^2 + w^2}{4}. \quad (4)$$

As each unit of case $\mathbb{T}$ in flat-folded state is connected along G_r, self-overlaps in flat-folded state can be avoided (Fig. 3h).

For units whose $w > h$ (Fig. 4a and b) we obtain an approximation with 'short' rectangular units (Fig. 4c). Guided by the mountain and valley folding creases, such an approximation is transformable but cannot reach the final flat-folded state caused by self-penetrations of each unit (Fig. 4d). Specifically, pair of vertices $C_2\hat{C}_6$in unit U^O; $D_1\hat{D}_6$ and $D_3\hat{D}_8$ in unit U^E may touch during folding. One could decrease w by increasing the number of columns N_c to let $w = h$ or $w < h$, such two cases have been discussed above. Instead, we modify the creases of units inspired by

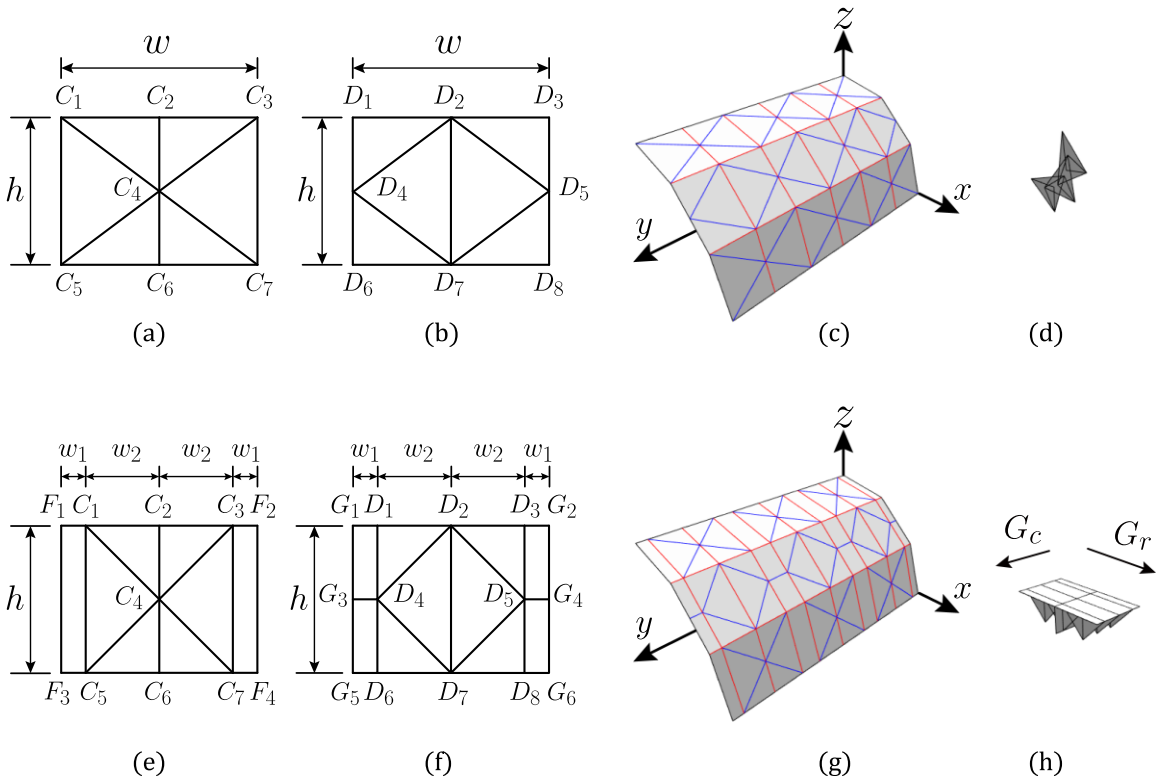

Figure 4: Cylindrical target surface approximation via rectangular units whose width w is greater than height h. (a) A 'short' rectangular unit $U^{\mathbb{O}}$ for tiling odd rows. (b) A 'short' rectangular unit $U^{\mathbb{E}}$ for tiling even rows. (c) The approximated origami structure composed of units $U^{\mathbb{O}}$ and $U^{\mathbb{E}}$. (d) The flat-folded state with self-penetrations. (e) A unit $U^{\mathbb{O}}$ of case $\mathbb{S}$ modified from the unit shown in (a). (f) A unit $U^{\mathbb{E}}$ of case $\mathbb{S}$ modified from the unit shown in (b). (g) The approximated origami structure via units $U^{\mathbb{O}}$ and $U^{\mathbb{E}}$ of case $\mathbb{S}$. (h) The fully folded state of the approximation shown in (g).

the work of Zhao *et al.* (2021), in which waterbomb-derivative tessellations with quad-paddings were demonstrated. For the unit $U^{\mathbb{O}}$ with modified creases (Fig. 4e), the size of rectangle $C_1C_3C_7C_5$ is changed from $w \times h$ to $2w_2 \times h$, where

$$w_2 = \frac{h}{2}.$$

The self-penetration between vertices C_2 and C_6 can be avoided. Two quads $F_1C_1C_5F_3$ and $C_3F_2F_4C_7$ with size $w_1 \times h$ are appended to fill the space of the original 'short' rectangular unit, where

$$w_1 = \frac{w-h}{2}.$$

The modification of creases for unit $U^{\mathbb{E}}$ (Fig. 4f) is similar to the way of modifying unit $U^{\mathbb{O}}$. After converting the size of $D_1D_3D_8D_6$ from $w \times h$ to $2w_2 \times h$, four quads $G_1D_1D_4G_3$, $D_3G_2G_4D_5$, $G_3D_4D_6G_5$, and $D_5G_4G_6D_8$ with width of w_1 and height of $\frac{h}{2}$ are appended. We term modified units $U^{\mathbb{O}}$ (Fig. 4e) and $U^{\mathbb{E}}$ (Fig. 4f) as case $\mathbb{S}$. Figure 4g demonstrates the origami approximation by using these modified units. Note that adjacent lines between each column are coplanar in the fully folded state, thus they have been eliminated. Although it cannot be flat-folded, the origami approximation is compactly foldable without self-penetrations among each unit (Fig. 4h). The fully folded shape expands along two growing directions G_r determined by N_r and G_c determined by N_c, which are orthogonal. Let G_r and G_c be parallel to x- and y-axes, respectively, and then the volume of AABB for the origami structure when fully folded is calculated as

$$V^{\mathbb{S}} = N_c(w-h)A^{\mathbb{S}}, \tag{5}$$

where $A^{\mathbb{S}}$, the area of AABB projected on the x–z plane, is equal to $A^{\mathbb{E}}$. By substituting $A^{\mathbb{E}}$ (Equation 3) into Equation (5), the volume is rewritten as follows:

$$V^{\mathbb{S}} = \frac{N_c(N_r+1)}{4}(w-h)h^2. \tag{6}$$

Note that we were inspired by the work of Zhao *et al.* (2021) for appending quad-paddings to waterbomb tessellations. However, their motivation is to expand the design variation. In contrast, our motivation is to avoid self-penetrations within units. The crease pattern of each unit is modified. Its width w is first narrowed to the same as h. Then, rectangles are filled to match the original region of the unit.

The fully folded structure is bondable between two parallel so-called skin-planes (Suto *et al.*, 2018), which has the potential to generate a sandwich-like structure. It can be observed that faces are lying on the top plane and merely vertices and edges with zero area touch the bottom plane. Such vertex- and edge-touched locations may weaken the attached skin-plane. To tackle this, we modify the creases based on case $\mathbb{S}$ as shown in Fig. 5. Width w_2' is introduced, that is

$$w_2' = \lambda w_2,$$

where $\lambda \in (0, 1)$ is a parameter for scaling. Width w_1' is then be calculated as

$$w_1' = \frac{w}{2} - w_2'.$$

Squares $C_1C_3C_7C_5$ and $D_1D_3D_8D_6$ in case $\mathbb{S}$ are converted to 'tall' rectangles determined by λ. Then, we modify the creases in rectangles $C_1C_3C_7C_5$ and $D_1D_3D_8D_6$ by splitting vertices with refer-

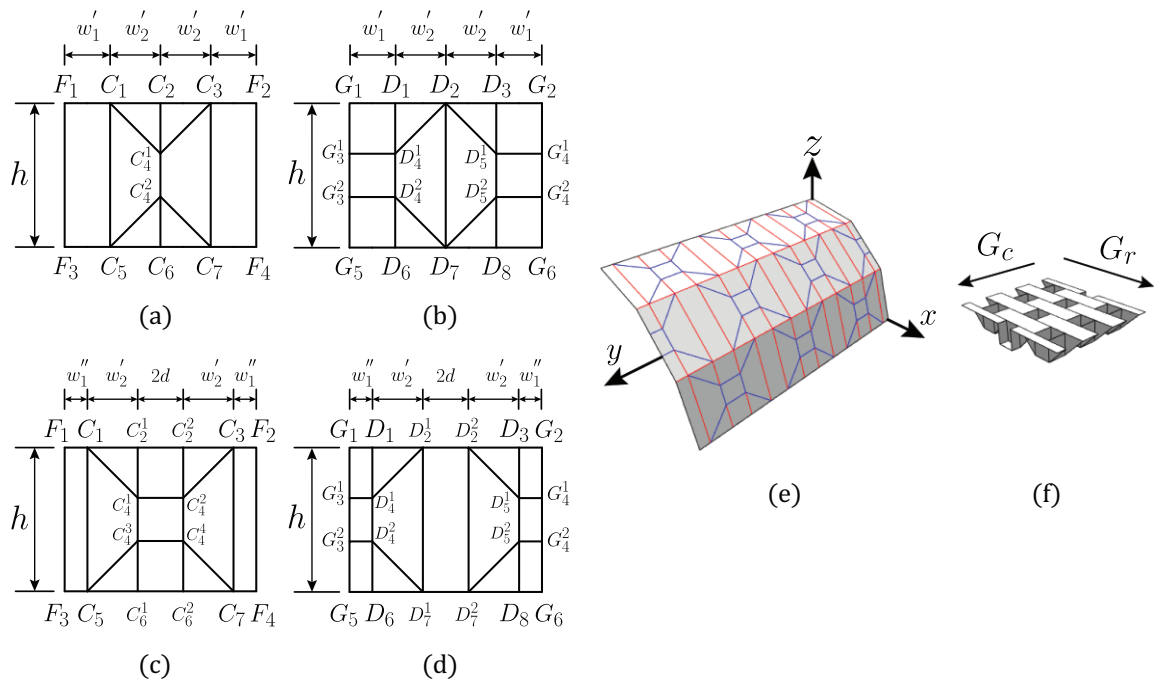

Figure 5: Cylindrical target surface approximation via rectangular units of case 𝕊II. (a) Modifying unit U^O of case 𝕊 with referring to the unit of case 𝕋. (b) Modifying unit U^E of case 𝕊 with referring to the unit of case 𝕋. (c) A unit U^O of case 𝕊II for tiling odd rows. (d) A unit U^E of case 𝕊II for tiling even rows. (e) An approximated origami structure via units U^O and U^E of case 𝕊II. (f) The fully folded state of the approximation shown in (e).

ring to the case 𝕋 (Fig. 5a and b). Since vertices D_4 and D_5 are respectively split into two vertices, two more quads $G_3^1D_4^1D_4^2G_3^2$ and $D_5^1G_4^1G_4^2D_5^2$ are appended. Next, we introduce a displacement parameter $d \in (0, w_1')$ to move the left of the middle part to the left and mirror-symmetrically move the right of the middle part to the right. Consequently as shown in Fig. 5c and d, one column is divided into five parts of lengths w_1'', w_2', $2d$, w_2', and w_1'', where

$$w_1'' = w_1' - d.$$

The modified units U^O (Fig. 5c) and U^E (Fig. 5d) are termed as case 𝕊II since they are modelled based on units of case 𝕊. Figure 5e and f, respectively, demonstrate the deployed and fully folded origami approximations consisting of such units, where λ is of 0.7 and d is of $\frac{w_1'}{2}$. The structure belongs to the face-bondable origami tessellation (Suto *et al.*, 2018) whose fully folded structure exists between two parallel planes to which faces of the origami approximation are touched. For the AABB, its area projected on the x–z plane can be calculated by referring to case 𝕋 using Equation (4) where w is set to λh. Correspondingly, the volume of the AABB is given in Equation (7).

$$V^{\mathbb{S}II} = N_c(w - \lambda h)\frac{2N_r - \lambda N_r + \lambda}{4}\lambda h^2. \tag{7}$$

4 Results

The proposed method allows the user to construct foldable cylindrical approximations via unified square or rectangular units with unfolded creases. An interactive design and exploration framework was written for implementing the proposed method. We collected all data in this paper on a laptop with an Intel(R) Core(TM) i5-9300H CPU and a 16-GB RAM.

4.1 Approximations via square units

As shown in Fig. 6, several origami approximations are demonstrated with units of case 𝔼 for fitting cylindrical target surfaces. Statistics of these obtained approximations are shown in Table 1. First, the user interactively specifies a profile curve Γ on the x–z plane according to the cylindrical target surface. Then, we divide such a curve into N_r segments with unified length of h via optimization. N_c is another parameter used to calculate $w = W/N_c$, where W is the width of the target. w could be less than, equal to, or greater than h. Thus cases 𝕋, 𝔼, and 𝕊 or 𝕊II could be utilized for approximation.

In our experimental configuration the width W of the target is set as $W = N_c w$, where $w = h$, to obtain the approximations based on units of case 𝔼. Later, for the same target specified by the curve Γ and width W, N_c is increased and decreased for generating unified rectangular units whose $w < h$ and $w > h$, respectively. In Fig. 6, the first five and last four approximations are generated by open and closed curves Γ, respectively. Such approximations, e.g. shelter, chair, rolling paper, mushroom, and whale, whose profile curve Γ is divided by small N_r, can still capture the general characteristics of the target and would make them easier for fabrication. The approximations with a large N_r, e.g. Fermat's spiral, capital omega, airfoil, and Stanford bunny, show the ability to maintain the detailed curved feature of the target but could involve more human labour during fabrication. We introduce $|\mathbf{R}_{max}|$ and $|\mathbf{R}_{ave}|$ to respectively demonstrate the maximum and average of absolute r_k, where k is ranging from 1 to N_r. Levenberg–Marquardt algorithm described in section 3.2 of Madsen *et al.* (2004) is imple-

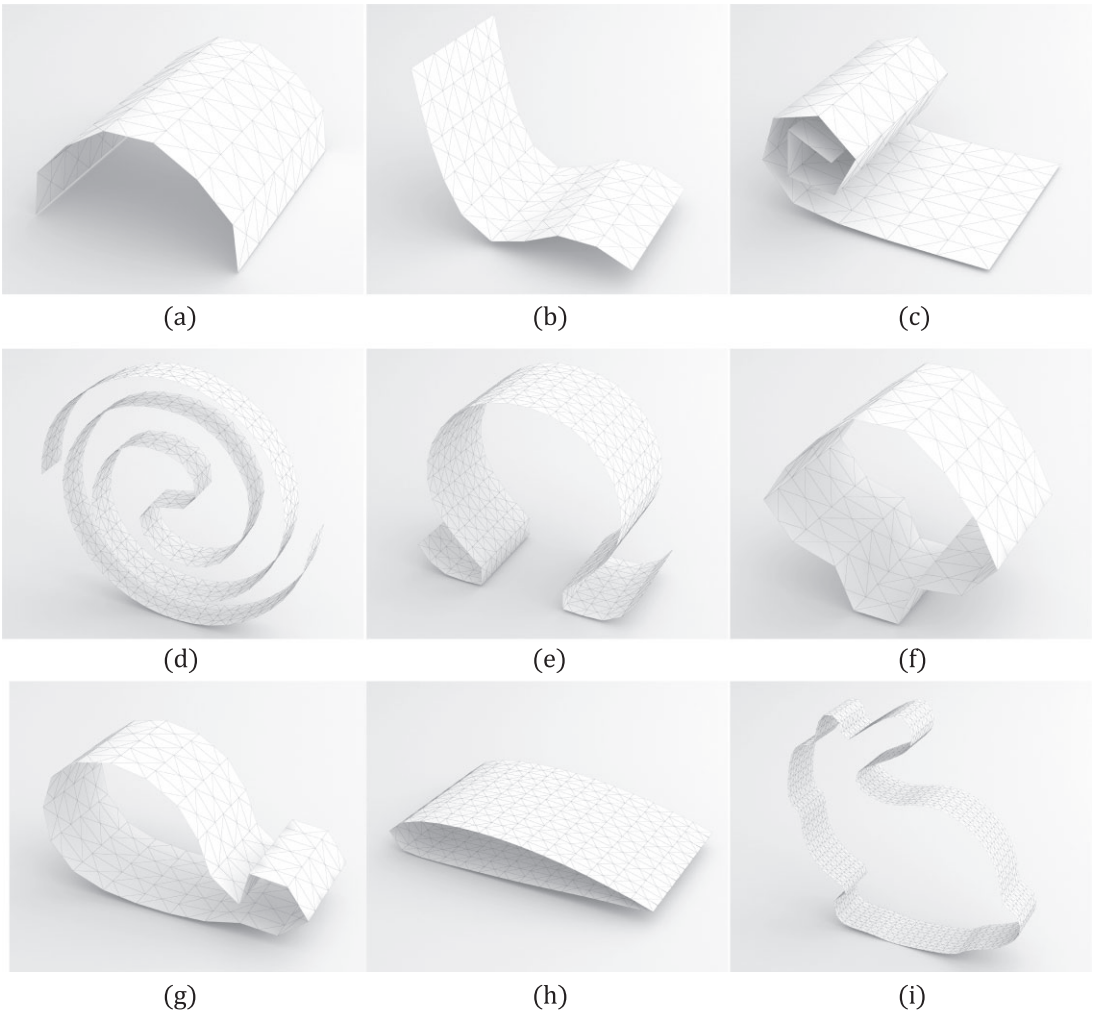

Figure 6: Resulting origami structures with units of case $\mathbb{E}$ for approximation. (a) Shelter. (b) Chair. (c) Rolling paper. (d) Fermat's spiral. (e) Capital omega. (f) Mushroom. (g) Whale. (h) Airfoil. (i) Stanford bunny.

Table 1: Statistics of approximations via units of case $\mathbb{E}$ shown in Fig. 6.

Models	$N_r \times N_c$	$\lvert R_{max}\rvert$ / $\lvert R_{ave}\rvert$	T (s)
(a)	7 × 5	2.62096e−14 / 8.61766e−15	0.010
(b)	9 × 4	1.95472e−14 / 9.99077e−15	0.033
(c)	12 × 4	7.28233e−14 / 2.64116e−14	0.088
(d)	100 × 2	2.73695e−11 / 3.98563e−12	39.268
(e)	35 × 5	5.03413e−13 / 1.56708e−13	1.475
(f)	14 × 3	1.06474e−13 / 2.58246e−14	0.208
(g)	20 × 3	1.40942e−12 / 2.89229e−13	0.351
(h)	26 × 7	6.06483e−13 / 1.00295e−13	0.534
(i)	100 × 5	7.24736e−11 / 9.98287e−12	56.024

mented for minimization. T is the time needed (in seconds) for optimization. The optimization is terminated when $|\mathbf{R}_{max}|$ is less than a threshold of 1.0e−12 or the number of iterations reaches a user-specified number of times. After optimization, h of each unit is unified to $\overline{h}$.

4.2 Approximations via non-square units

The units of case $\mathbb{E}$ whose $w = h$ may limit the application scenarios. Together with the origami approximations via units of case $\mathbb{E}$, we demonstrate approximations via units of cases $\mathbb{T}$, $\mathbb{S}$, and $\mathbb{S}$II in Figs 7 and 8. In each case, the deployed and fully folded states are shown at left and right, respectively. The number of units $N_r \times N_c$ for each origami structure is shown in Table 2. Note that we utilize the same N_r to divide the profile curve Γ for all cases. Based on the origami approximation using units of case $\mathbb{E}$, we increase N_c to conduct units of case $\mathbb{T}$ and decrease N_c to generate units of cases $\mathbb{S}$ and $\mathbb{S}$II.

4.3 Fabrications

We demonstrate fabricated origami approximations of the shelter in Fig. 9. In each row, origami structure in deployed state, fully compact state, its corresponding fabrication of deployed state, and fabrication of fully compact state are presented from left to right, respectively. Sketch papers were utilized as the fabricating materials. A Silhouette CAMEO cutting machine (Silhouette America, Inc.) was adopted for cutting out crease patterns.

5 Discussion

Cylindrical target surfaces generated by previous origami-inspired approaches are mostly based on Miura-ori (Wang *et al.*, 2016; Hu *et al.*, 2019; Du *et al.*, 2021) and waterbomb tessellations (Zhao *et al.*, 2021). The outline of the target is captured; however,

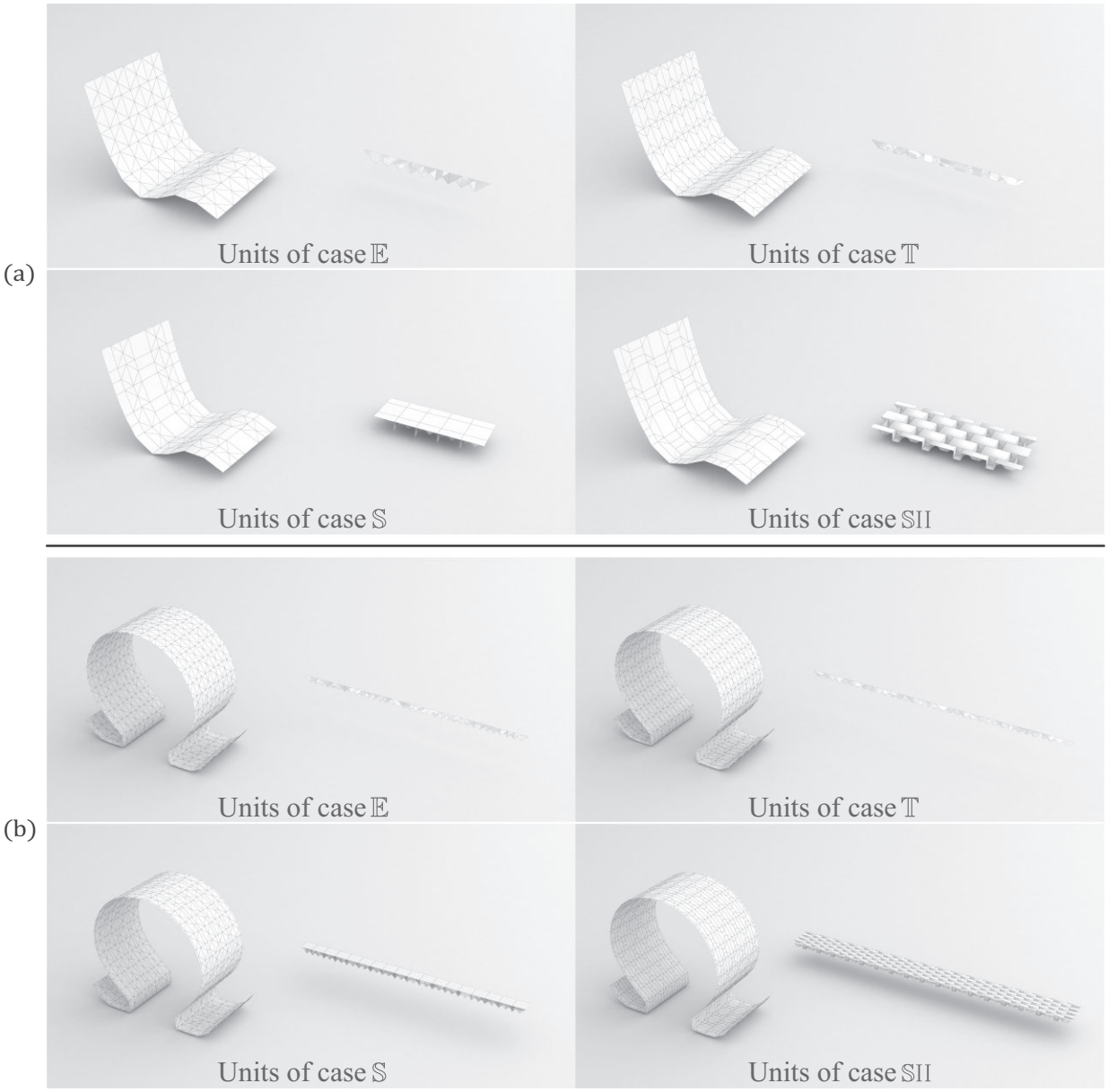

Figure 7: Resulting origami approximations with open profile curve Γ. (a) Approximations for chair. (b) Approximations for capital omega. In each result, we demonstrate the origami approximations via units of cases $\mathbb{E}$, $\mathbb{T}$, $\mathbb{S}$, and $\mathbb{S}$II, respectively. In each case, the deployed and fully folded states are shown from left to right, respectively.

the corrugated surface caused by folding all creases would be inconvenient for application scenarios requiring a 'smooth' surface, e.g. the surfaces of a shelter and an airfoil require rain and airflow easily pass through. In our work, the cylindrical target surface is constructed by a set of unified square or rectangular units with unfolded creases. The constructed structure can be interpreted as a discrete version of the target surface. Furthermore, the deployed structure can still be folded to a compact state when folding all creases.

Tang *et al.* approximated revolutionary surfaces by using unfolded waterbomb bases (Tang *et al.*, 2021), which is more relevant to our work. Due to the geometric difference between the revolutionary and the cylindrical surfaces, the crease pattern generated in their work needs to be divided into several parts while the crease pattern satisfies developability in our work. In addition, variations of the waterbomb tessellation are utilized in our work for approximation and a type of face-bondable origami structure is demonstrated.

We discretize the profile curve Γ into N_r segments through optimization for unifying the length of each segment. Then, the target surface is tiled with unified units which could realize cost-efficient constructions for origami structures that are assembled by a large number of units required to be made individually. Although the error between N_r segments and the curve can be further minimized based on another division strategy such as Douglas–Peucker algorithm (Douglas & Peucker, 1973), the lengths of the segments could be varied. For a given width w of one column (Fig. 10a), various segment lengths could lead to square ($w = h$), tall ($w < h$), and short ($w > h$) units. As presented previously, the tall unit would be flat-folded to a curved outline which may cause

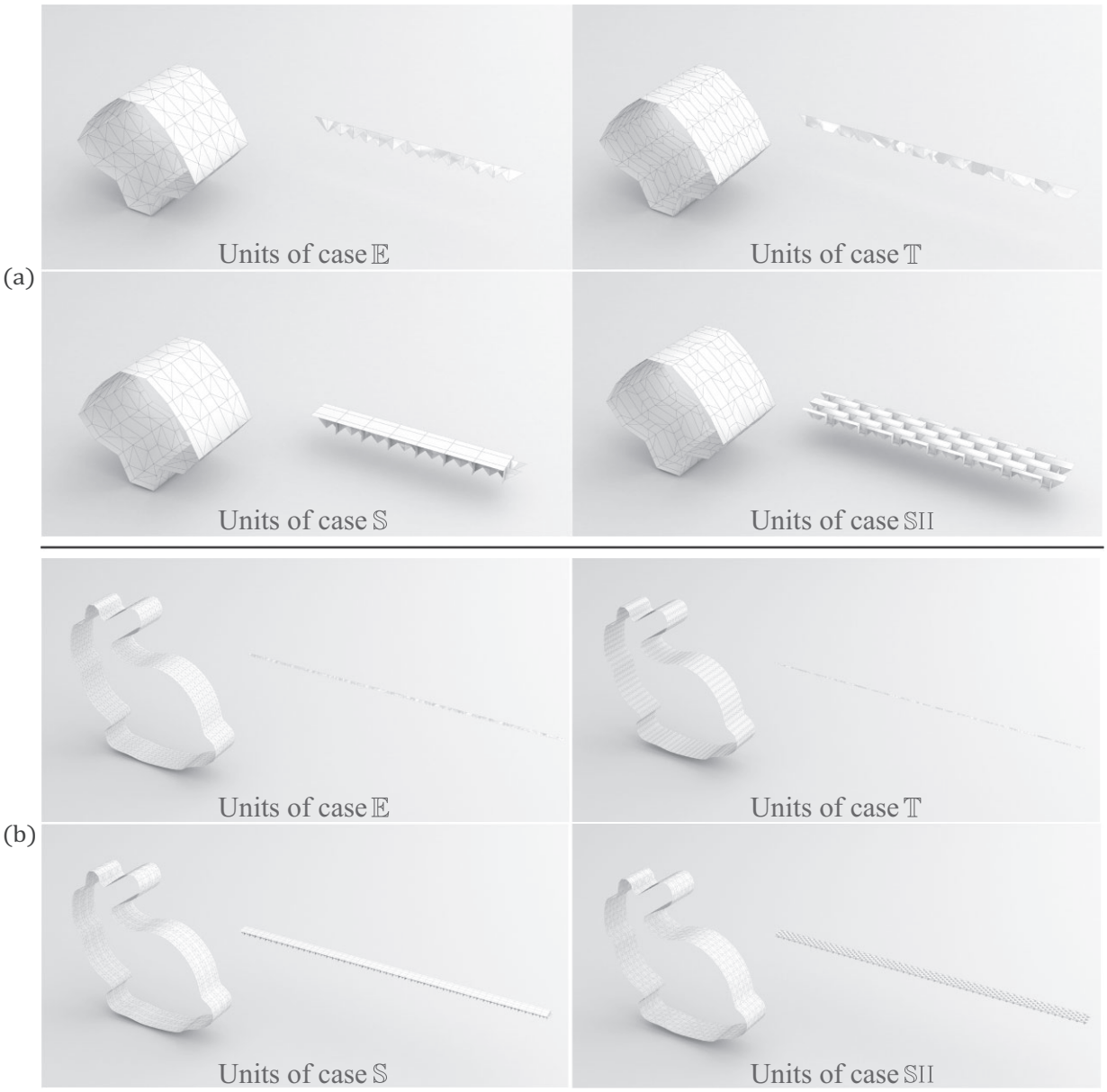

Figure 8: Resulting origami approximations with closed profile curve Γ. (a) Approximations for mushroom. (b) Approximations for Stanford bunny. In each result, the origami approximations via units of cases $\mathbb{E}$, $\mathbb{T}$, $\mathbb{S}$, and $\mathbb{S}$II are demonstrated, respectively. In each case, the deployed and fully folded states are shown at left and right, correspondingly.

Table 2: The number of units $N_r \times N_c$ for origami approximations.

Models	Case $\mathbb{E}$	Case $\mathbb{T}$	Cases $\mathbb{S}$ and $\mathbb{S}$II
Fig. 7a	9 × 4	9 × 6	9 × 2
Fig. 7b	35 × 5	35 × 6	35 × 4
Fig. 8a	14 × 3	14 × 5	14 × 2
Fig. 8b	100 × 5	100 × 8	100 × 3

self-overlaps and the short unit cannot be fully folded caused by self-penetrations. Based on crease modification self-overlaps of the tall unit can be avoided. However, creases of the short unit after modification could be incompatible with the creases of the adjacent units (Fig. 10b).

Map folding (Lunnon, 1971) folds a flat sheet with $N_r \times N_c$ units into a compact state with 1×1 unit. By unifying the composed units, we uncover a connection between the resulting origami structures and the way of map folding. In particular, creases inside each unit can be disabled and creases between adjacent units are folded with referring to the map folding for generating a more compact state if needed. Through folding selected creases to achieve various shapes can also be found in the work of Hawkes *et al.* (2010), in which a shape-shifting robot was developed. The method proposed here cannot only fold the deployed structure to a fully compact state with the prescribed region of AABB, but also show the possibility of map folding based on the foundation of unified units.

Yamamoto and Mitani demonstrated an example of the Miura-ori whose facets are replaced by connecting shrinkable patterns

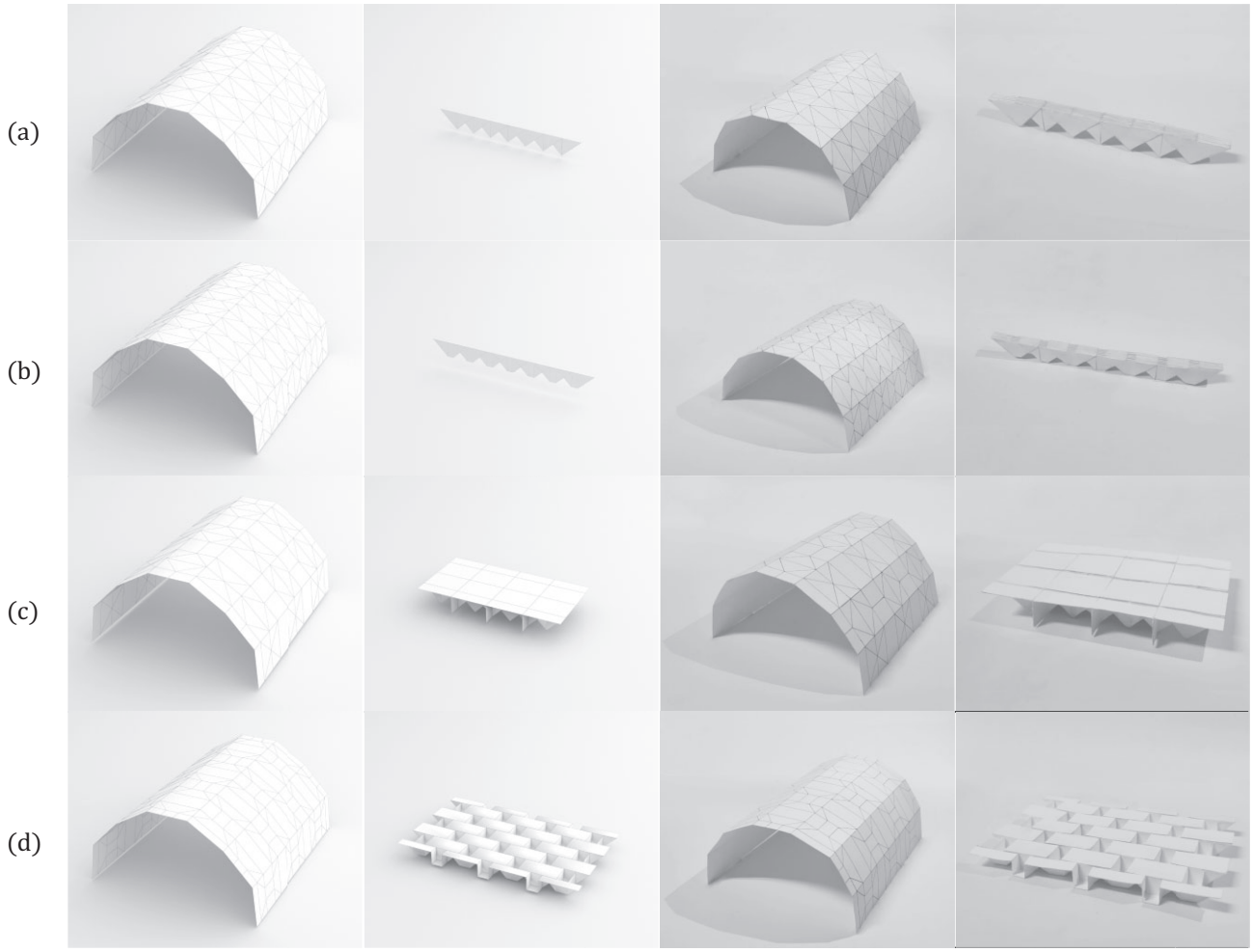

Figure 9: Fabrications of shelter. (a) Fabrication via units of case $\mathbb{E}$. (b) Fabrication via units of case $\mathbb{T}$. (c) Fabrication via units of case $\mathbb{S}$. (d) Fabrication via units of case $\mathbb{SII}$. In each result, origami structure in deployed state, fully compact state, fabrication of deployed state, and fabrication of fully compact state are presented at left and right, respectively.

(Yamamoto & Mitani, 2022). Later, an origami tessellation hole problem was redefined and solved based on triangle twist folding (Yamamoto *et al.*, 2022). Utilizing such shrinkable patterns to the waterbomb tessellation could expand the existing patterns and would be an interesting topic for future study.

One apparent limitation of the proposed method is that it only handles the approximation of cylindrical surfaces. The approximation strategy of folding a portion of creases and keeping the rest creases unfolded limits the design space. The underlying geometry is the waterbomb tessellation, we conjecture that if all creases are appropriately folded, versatile structures would be constructed based on recently proposed methods for approximating developable waterbomb origami structures (Zhao *et al.*, 2018b) and designing cylindrical and axisymmetric waterbomb tessellations (Zhao *et al.*, 2021).

6 Conclusions

In this paper, we proposed a method for constructing cylindrical target surfaces consisting of unified square or rectangular units with crease patterns inspired by the waterbomb tessellation. The appearance of the target can be flexibly approximated for the satisfaction of the application-specific requirements. The origami structure is deployed by folding a portion of creases and can still be compactly stored by folding all creases. In addition, we analysed various relationships between the width and height of the elemental units and utilized variations of the waterbomb tessellations to control the region of the origami structure when fully folded. Our work could potentially be applied in the fields, such as aerospace, robotics, metamaterials, and so on.

Future work contains a full investigation of the continuous folding motion for the demonstrated variations of the waterbomb tessellation. Currently, we only adopt the 'Origami Simulator' (Ghassaei *et al.*, 2018), a simple and effective mass-spring-damper-based simulator, to visualize the folding process (Appendix A). Further study on the exploration of applying the demonstrated variations of the waterbomb tessellation in partially folded states to approximate versatile target surfaces is also planned.

Acknowledgments

This work was supported by the National Natural Science Foundation of China (No. 61902155) and Research Initiation Fund for Senior Talents of Jiangsu University by Senior Talent Foundation of Jiangsu University (No. 19JDG024).

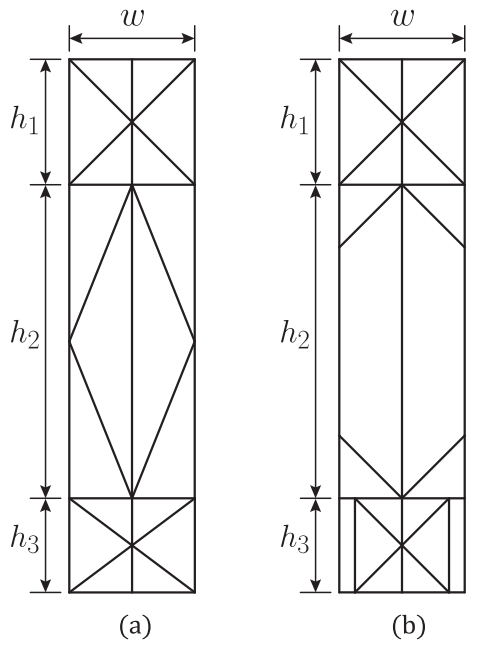

Figure 10: Dividing segments with vary lengths. (a) One column contains three units, where $w = h_1$, $w < h_2$, and $w > h_3$. (b) Crease modification for such a column. The middle unit is converted to case $\mathbb{T}$. The bottom unit is converted to case $\mathbb{S}$, which is not compatible with the adjacent unit.

Conflict of interest statement

None declared.

References

Dang, X., Feng, F., Plucinsky, P., James, R. D., Duan, H., & Wang, J. (2022). Inverse design of deployable origami structures that approximate a general surface. *International Journal of Solids and Structures*, **234**, 111224. https://doi.org/10.1016/j.ijsolstr.2021.111224.

Demaine, E. D., & O'Rourke, J. (2007). *Geometric folding algorithms: Linkages, origami, polyhedra*. Cambridge University Press.

Demaine, E. D., & Tachi, T. (2017). Origamizer: A practical algorithm for folding any polyhedron. In *Proceedings of the Leibniz International Proceedings in Informatics (LIPIcs)* (Vol. **77**, pp. 1–16). Schloss Dagstuhl-Leibniz-Zentrum fuer Informatik.

Dey, S., Fan, C., Gothelf, K. V., Li, J., Lin, C., Liu, L., Liu, N., Nijenhuis, M. A., Saccà, B., Simmel, F. C., Yan, H., & Zhan, P. (2021). DNA origami. *Nature Reviews Methods Primers*, **1**(1), 1–24. https://doi.org/10.1038/s43586-020-00009-8.

Douglas, D. H., & Peucker, T. K. (1973). Algorithms for the reduction of the number of points required to represent a digitized line or its caricature. *Cartographica: The International Journal for Geographic Information and Geovisualization*, **10**(2), 112–122. https://doi.org/10.3138/FM57-6770-U75U-7727.

Du, Y., Keller, T., Song, C., Xiao, Z., Wu, L., & Xiong, J. (2021). Design and foldability of Miura-based cylindrical origami structures. *Thin-Walled Structures*, **159**, 107311. https://doi.org/10.1016/j.tws.2020.107311.

Dudte, L. H., Vouga, E., Tachi, T., & Mahadevan, L. (2016). Programming curvature using origami tessellations. *Nature Materials*, **15**(5), 583–588. https://doi.org/10.1038/nmat4540.

Dudte, L. H., Choi, G. P., & Mahadevan, L. (2021). An additive algorithm for origami design. *Proceedings of the National Academy of Sciences*, **118**(21), e2019241118. https://doi.org/10.1073/pnas.2019241118.

Feng, H., Ma, J., Chen, Y., & You, Z. (2018). Twist of tubular mechanical metamaterials based on waterbomb origami. *Scientific Reports*, **8**(1), 9522. https://doi.org/10.1038/s41598-018-27877-1.

Ghassaei, A., Demaine, E. D., & Gershenfeld, N. (2018). Fast, interactive origami simulation using GPU computation. *Origami*, **7**, 1151–1166.

Hawkes, E., An, B., Benbernou, N. M., Tanaka, H., Kim, S., Demaine, E. D., Rus, D., & Wood, R. J. (2010). Programmable matter by folding. *Proceedings of the National Academy of Sciences*, **107**(28), 12441–12445. https://doi.org/10.1073/pnas.0914069107.

Hu, Y., Liang, H., & Duan, H. (2019). Design of cylindrical and axisymmetric origami structures based on generalized Miura-ori cell. *Journal of Mechanisms and Robotics*, **11**(5), 051004. https://doi.org/10.1115/1.4043800.

Kuribayashi, K., Tsuchiya, K., You, Z., Tomus, D., Umemoto, M., Ito, T., & Sasaki, M. (2006). Self-deployable origami stent grafts as a biomedical application of Ni-rich tini shape memory alloy foil. *Materials Science and Engineering: A*, **419**(1), 131–137. https://doi.org/10.1016/j.msea.2005.12.016.

Lee, T.-U., Liu, Y., & Xie, Y. M. (2022). Dividing a sphere hierarchically into a large number of spherical pentagons using equal area or equal length optimization. *Computer-Aided Design*, **148**, 103259. https://doi.org/10.1016/j.cad.2022.103259.

Lunnon, W. (1971). Multi-dimensional map-folding. *The Computer Journal*, **14**(1), 75–80. https://doi.org/10.1093/comjnl/14.1.75.

Madsen, K., Nielsen, H. B., & Tingleff, O. (2004). Methods for non-linear least squares problems. (2nd ed.). Informatics and Mathematical Modelling, Technical University of Denmark.

Melancon, D., Gorissen, B., García-Mora, C. J., Hoberman, C., & Bertoldi, K. (2021). Multistable inflatable origami structures at the metre scale. *Nature*, **592**(7855), 545–550. https://doi.org/10.1038/s41586-021-03407-4.

Pehrson, N. A., Ames, D. C., Smith, S. P., Magleby, S. P., & Arya, M. (2020). Self-deployable, self-stiffening, and retractable origami-based arrays for spacecraft. *AIAA Journal*, **58**(7), 3221–3228. https://doi.org/10.2514/1.J058778.

Pérez, F., & Suárez, J. A. (2007). Quasi-developable B-spline surfaces in ship hull design. *Computer-Aided Design*, **39**(10), 853–862. https://doi.org/10.1016/j.cad.2007.04.004.

Schenk, M., Viquerat, A. D., Seffen, K. A., & Guest, S. D. (2014). Review of inflatable booms for deployable space structures: Packing and rigidization. *Journal of Spacecraft and Rockets*, **51**(3), 762–778. https://doi.org/10.2514/1.A32598.

Sharma, H., & Upadhyay, S. (2021). Folding pattern design and deformation behavior of origami based conical structures. *Advances in Space Research*, **67**(7), 2058–2076. https://doi.org/10.1016/j.asr.2021.01.012.

Suto, K., Adachi, A., Tachi, T., & Yamaguchi, Y. (2018). An edge extrusion-approach to generate extruded Miura-ori and its double tiling origami patterns. arXiv preprint arXiv:1810.04625. https://doi.org/10.48550/arXiv.1810.04625.

Tachi, T. (2009). 3D origami design based on tucking molecule. In *Origami 4* (pp. 271–284), AK Peters/CRC Press.

Tachi, T. (2010a). Freeform variations of origami. *Journal for Geometry and Graphics*, **14**(2), 203–215.

Tachi, T. (2010b). Origamizing polyhedral surfaces. *IEEE Transactions on Visualization and Computer Graphics*, **16**(2), 298–311. https://doi.org/10.1109/TVCG.2009.67.

Tachi, T. (2013). Designing freeform origami tessellations by generalizing Resch's patterns. *Journal of Mechanical Design*, **135**(11), 111006. https://doi.org/10.1115/1.4025389.

Tang, J., Tian, M., Wang, C., Wang, X., & Mao, H. (2021). A novel scheme of folding discretized surfaces of revolution inspired by waterbomb origami. *Mechanism and Machine Theory*, **165**, 104431. https://doi.org/10.1016/j.mechmachtheory.2021.104431.

Wang, F., Gong, H., Chen, X., & Chen, C. (2016). Folding to curved surfaces: A generalized design method and mechanics of origami-based cylindrical structures. *Scientific Reports*, **6**(1), 1–10. https://doi.org/10.1038/srep33312.

Yamamoto, Y., & Mitani, J. (2022). Shrinkable self-similar structure design. *Journal of Mechanisms and Robotics*, **14**(4), 041003. https://doi.org/10.1115/1.4053528.

Yamamoto, Y., Nakazato, R., & Mitani, J. (2022). Method for solving origami tessellation hole problem using triangle twist folding. *Journal of Computational Design and Engineering*, **9**(1), 144–154. https://doi.org/10.1093/jcde/qwab074.

Yasuda, H., Tachi, T., Lee, M., & Yang, J. (2017). Origami-based tunable truss structures for non-volatile mechanical memory operation. *Nature communications*, **8**(1), 1–7. https://doi.org/10.1038/s41467-017-00670-w.

Zhao, Y., Kanamori, Y., & Mitani, J. (2017). Geometry of axisymmetric 3D origami consisting of triangular facets. *Journal for Geometry and Graphics*, **21**(1), 107–118.

Zhao, Y., Endo, Y., Kanamori, Y., & Mitani, J. (2018a). A computational design method for tucking axisymmetric origami consisting of triangular facets. *Symmetry*, **10**(10), 469. https://doi.org/10.3390/sym10100469.

Zhao, Y., Endo, Y., Kanamori, Y., & Mitani, J. (2018b). Approximating 3D surfaces using generalized waterbomb tessellations. *Journal of Computational Design and Engineering*, **5**, 442–448. https://doi.org/10.1016/j.jcde.2018.01.002.

Zhao, Y., Kanamori, Y., & Mitani, J. (2018c). Design and motion analysis of axisymmetric 3D origami with generic six-crease bases. *Computer Aided Geometric Design*, **59**, 86–97. https://doi.org/10.1016/j.cagd.2017.10.002.

Zhao, Y., Li, S., Zhang, M., Zeng, L., Yang, Y., Kanamori, Y., & Mitani, J. (2021). Computational design methods for cylindrical and axisymmetric waterbomb tessellations. *Computer Aided Geometric Design*, **91**, 102037. https://doi.org/10.1016/j.cagd.2021.102037.

Appendix 1. Folding Motions

Current work only demonstrates the deployed and fully folded states of the origami structure but ignores the intermediate states. To better understand the folding process, we divide it into two stages, i.e., firstly transforming the deployed structure to the unfolded planar shape and secondly folding the planar shape to the fully folded structure in a way similar to the folding of a waterbomb tessellation. Here, we demonstrate such folding sequences via 'Origami Simulator' (Ghassaei *et al.*, 2018) in Fig. A1. A full investigation of the continuous folding motion is an interesting topic and would be a topic for future study.

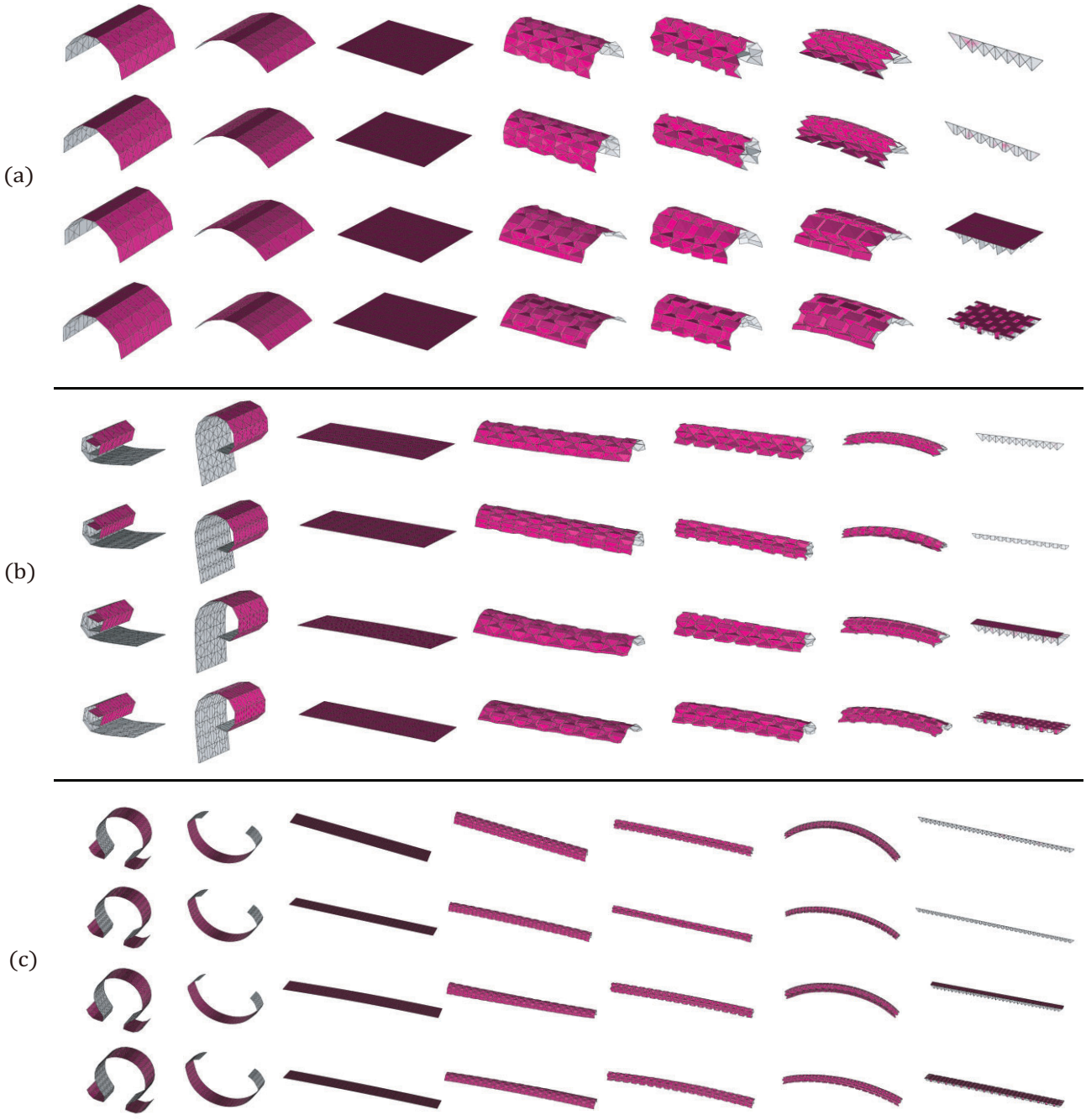

Figure A1. Folding sequences of origami approximations via units of cases 𝔼, 𝕋, 𝕊, and 𝕊II. (a) Folding sequences of shelter. (b) Folding sequences of rolling paper. (c) Folding sequences of capital omega. In each result, origami approximations are based on units of cases 𝔼, 𝕋, 𝕊, and 𝕊II, respectively, from top to bottom. The origami structure in the deployed state is firstly transformed to the planar state. Then, the planar state is folded to the fully compact state.